27 September 2013 | $10

Science

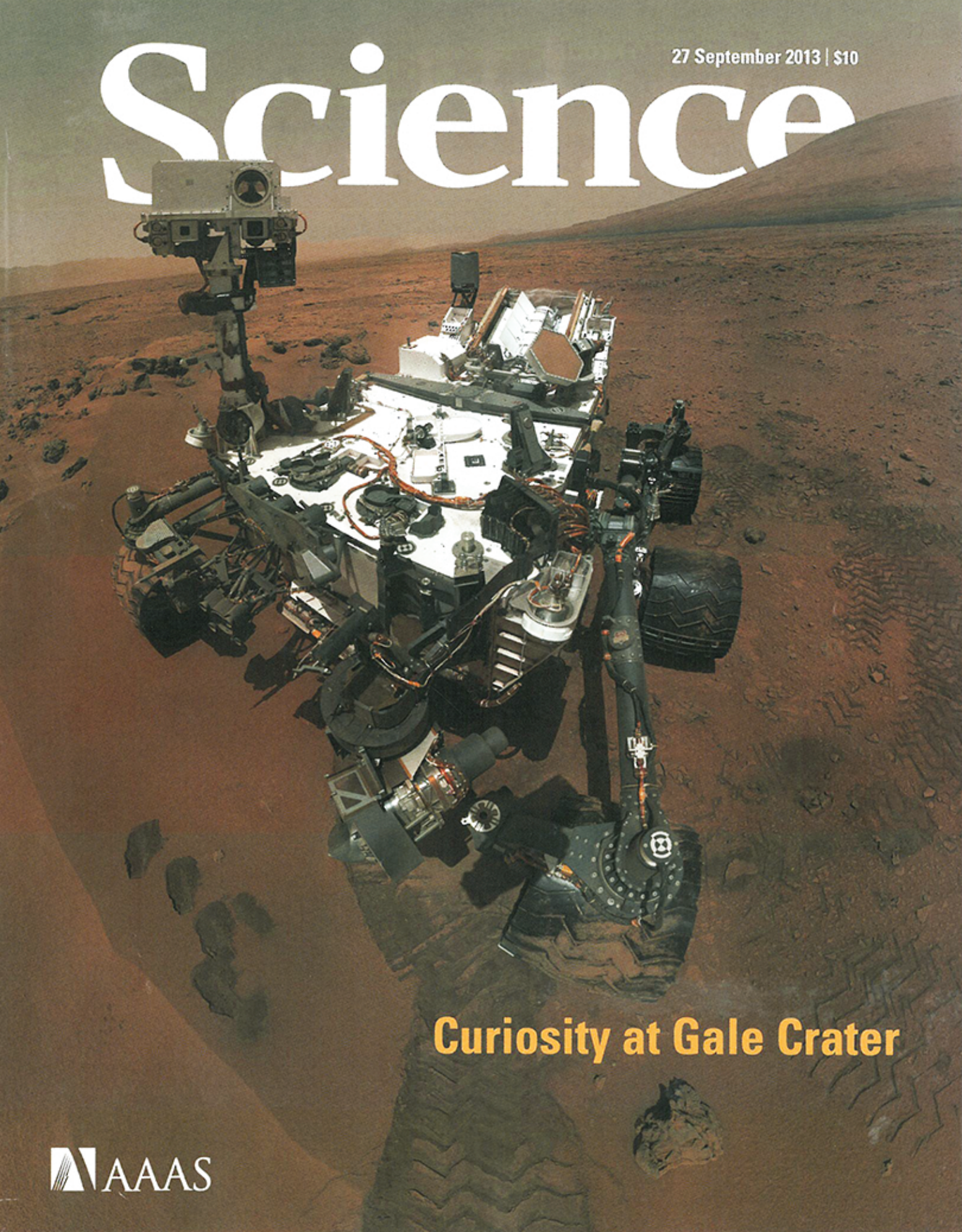

Curiosity at Gale Crater

AAAS

Volatile, Isotope, and Organic Analysis of Martian Fines with the Mars Curiosity Rover

L. A. Leshin *et al.*

Science **341**, (2013);
DOI: 10.1126/science.1238937

Volatile, Isotope, and Organic Analysis of Martian Fines with the Mars Curiosity Rover

L. A. Leshin,[1]* P. R. Mahaffy,[2] C. R. Webster,[3] M. Cabane,[4] P. Coll,[5] P. G. Conrad,[2] P. D. Archer Jr.,[6] S. K. Atreya,[7] A. E. Brunner,[2,8] A. Buch,[9] J. L. Eigenbrode,[2] G. J. Flesch,[3] H. B. Franz,[2,10] C. Freissinet,[2] D. P. Glavin,[2] A. C. McAdam,[2] K. E. Miller,[11] D. W. Ming,[6] R. V. Morris,[6] R. Navarro-González,[12] P. B. Niles,[6] T. Owen,[13] R. O. Pepin,[14] S. Squyres,[15] A. Steele,[16] J. C. Stern,[2] R. E. Summons,[11] D. Y. Sumner,[17] B. Sutter,[6,18] C. Szopa,[4] S. Teinturier,[4] M. G. Trainer,[2] J. J. Wray,[19] J. P. Grotzinger,[20] MSL Science Team†

Samples from the Rocknest aeolian deposit were heated to ~835°C under helium flow and evolved gases analyzed by Curiosity's Sample Analysis at Mars instrument suite. H_2O, SO_2, CO_2, and O_2 were the major gases released. Water abundance (1.5 to 3 weight percent) and release temperature suggest that H_2O is bound within an amorphous component of the sample. Decomposition of fine-grained Fe or Mg carbonate is the likely source of much of the evolved CO_2. Evolved O_2 is coincident with the release of Cl, suggesting that oxygen is produced from thermal decomposition of an oxychloride compound. Elevated δD values are consistent with recent atmospheric exchange. Carbon isotopes indicate multiple carbon sources in the fines. Several simple organic compounds were detected, but they are not definitively martian in origin.

The exchange of materials between a planet's interior, surface, and atmosphere drives the composition of mineral and chemical constituents that can create habitable environments on the terrestrial planets. Surface deposits, including aeolian fines, form an important record of these material exchanges. Martian surface fines are especially interesting because previous chemical studies by the Viking landers, Pathfinder, Spirit, and Opportunity (*1*–*4*) show that the bulk chemical composition of these materials is relatively constant at widely spaced locations across the planet. This can result from a combination of mechanical mixing on global scales and a similarity in the chemical composition of bedrock and sediments on regional to global scales (*5*). The finer-grained fractions, in particular, may provide information about the average composition of the martian crust (*6*).

The Sample Analysis at Mars (SAM) instrument suite onboard the Mars Science Laboratory (MSL) rover Curiosity provides diverse analytical capabilities for exploring martian materials, including volatile and isotopic compositions, and a search for organic compounds, whether of abiotic or biological origin (*7*). Traces of organic compounds have been found in martian meteorites (*8*–*12*), but previous landed missions, most notably Viking, did not find definitive evidence of martian organic material (*13*).

Curiosity's first sampling campaign took place at Rocknest, an aeolian sand shadow. The rover ingested fine-grained Rocknest material into its two analytical instruments: Chemistry and Mineralogy (CheMin), for x-ray diffraction, and SAM, for analysis of volatiles. Both SAM and CheMin sampled portions from scooped materials that were sieved to contain grain sizes <150 μm. Mineralogical and chemical results summarized in a companion paper (*14*) indicate bulk composition similar to martian fines analyzed by previous missions. Plagioclase, olivine, augite, pigeonite, and minor magnetite are the major igneous minerals (*15*). Minor anhydrite and hematite are the only nonigneous minerals detected. Along with these crystalline phases, the chemical and mineralogical analyses indicate that almost half of the <150-μm fraction comprises amorphous material (*14*). SAM performs evolved gas analysis (EGA) with the quadrupole mass spectrometer (QMS) and isotope measurements of evolved gases using both the QMS and the tunable laser spectrometer (TLS), the latter being sensitive to isotopes of CO_2 and H_2O. Organic analyses can be performed with the QMS alone or when it is coupled to the gas chromatograph (GC). SAM analyzed four separate portions from the fifth scooped sample at Rocknest

Table 1. Experiment parameters for four analyses of Rocknest fines. All evolved gases were analyzed by the QMS; temperature (*T*) range of gases that were then sent to the GC and TLS are shown.

Rocknest run	Sol (mission day)	Sample T range of gas sent to GC (°C)	Sample T range of gas sent to TLS (°C)	Rationale
Run 1	93	146–533	547–702*	GC: Low-T organics TLS: Predicted T for thermal decomposition of carbonates
Run 2	96	98–425	440–601	GC: Low-T organics below SO_2 evolution T TLS: Target CO_2 from suspected carbonate peak
Run 3	99	533–822	234–425	GC: High-T organics TLS: Low-T CO_2 and H_2O evolution
Run 4	117	251–289	350–443	GC: Narrow T cut for organics below O_2 evolution T TLS: Narrow T cut targeting suspected carbonate

*Due to the low volume of gas released by Rocknest in this temperature range, isotope data were not obtained for this run.

[1]Department of Earth and Environmental Sciences and School of Science, Rensselaer Polytechnic Institute, Troy, NY 12180, USA. [2]Planetary Environments Laboratory, NASA Goddard Space Flight Center, Greenbelt MD 20771, USA. [3]Jet Propulsion Laboratory, California Institute of Technology, Pasadena, CA 91109, USA. [4]LATMOS, UPMC Univ. Paris 06, Université Versailles St-Quentin, UMR CNRS 8970, 75005 Paris, France. [5]LISA, Univ. Paris-Est Créteil, Univ. Paris Diderot and CNRS, 94000 Créteil, France. [6]Astromaterials Research and Exploration Science Directorate, NASA Johnson Space Center, Houston, TX 77058, USA. [7]Department of Atmospheric, Oceanic and Space Sciences, University of Michigan, Ann Arbor, MI 48109–2143, USA. [8]Department of Astronomy, University of Maryland, College Park, MD 20742, USA. [9]Laboratoire Génie des Procédés et Matériaux, Ecole Centrale Paris, 92295 Chatenay-Malabry, France. [10]Center for Research and Exploration in Space Science and Technology, University of Maryland Baltimore County, Baltimore, MD 21250, USA [11]Department of Earth, Atmospheric and Planetary Sciences, Massachusetts Institute of Technology, Cambridge, MA 02139, USA. [12]Instituto de Ciencias Nucleares, Universidad Nacional Autónoma de México, Ciudad Universitaria, México D.F. 04510, Mexico. [13]Institute for Astronomy, University of Hawaii, Honolulu, HI 96822, USA. [14]School of Physics and Astronomy, University of Minnesota, Minneapolis, MN 55455, USA. [15]Department of Astronomy, Cornell University, Ithaca, NY 14853, USA. [16]Geophysical Laboratory, Carnegie Institution of Washington, Washington, DC 20015, USA. [17]Department of Geology, University of California, Davis, CA 95616, USA. [18]Jacobs, Houston, TX 77058, USA. [19]School of Earth and Atmospheric Sciences, Georgia Institute of Technology, Atlanta, GA 30332, USA. [20]Division of Geological and Planetary Sciences, California Institute of Technology, Pasadena, CA 91125, USA.

*Corresponding author. E-mail: leshin@rpi.edu
†MSL Science Team authors and affiliations are listed in the supplementary materials.

(see Table 1 and Materials and Methods). The exact mass of each Rocknest portion delivered to SAM is not measured by Curiosity, but tests on Earth are consistent with 50 ± 8 mg per portion (*16*).

Results and Discussion

Volatile Release

The volatile compounds observed in EGA typically reflect a combination of processes including desorption of trapped volatiles, mineral thermal decomposition, and chemical reaction during heating of the samples (*17*, *18*). Pure minerals and chemicals produce volatile products at predictable temperatures; however, in natural mixtures, these temperatures can be strongly shifted by physical characteristics of the samples (e.g., grain size) and by interactions between mineral and chemical components (*17*).

All four Rocknest analyses yielded H_2O, SO_2, CO_2, and O_2, in descending order of average abundance (Fig. 1 and Table 2). H_2O, CO_2, and O_2 abundances are relatively consistent from run to run and track each other within experimental uncertainty, whereas SO_2 abundance is variable from run to run. Repeated observation of H_2O, CO_2, and O_2 gas abundances with similar values suggests that differences in sample mass cannot explain the heterogeneity in SO_2 abundance, and thus the variability must be due to variation in the abundance of S-bearing minerals in different portions.

The H_2O observed in Rocknest EGA comprises a broad peak centered at ~300°C. Abundance estimates are ~1.5 to 3 weight percent (wt %) H_2O in the <150-μm fraction. The peak temperature and breadth of the H_2O release is most consistent with bound H_2O in amorphous phases. Specifically, adsorbed H_2O, H_2O bound to amorphous phases (e.g., amorphous aluminosilicate materials, nanophase ferric oxides and oxyhydroxides), interlayer H_2O from phyllosilicates, dehydration of several salts, and dehydration of ferric oxyhydroxides could have contributed to the lower-temperature H_2O release (Fig. 2). Higher-temperature H_2O could result from more tightly bound structural H_2O and/or OH in minor minerals present below the CheMin detection limit, as well as H_2O occluded in minerals and glasses. However, if the water detected was released from a single host mineral, CheMin should have detected that host mineral. The lack of observed hydrous crystalline phases in the <150-μm fraction (*15*) implies that H_2O/OH is derived from the amorphous component. H_2O concentrations in the amorphous component are estimated to be 3 to 6 wt % H_2O.

Unlike the situation for H_2O, calculated abundances of carbonate inferred from CO_2 released, sulfate minerals from SO_2, and oxychloride compounds (e.g., chlorate or perchlorate) from O_2 would all be at or below the detection limits of CheMin, affirming the complementarity of SAM and CheMin on Curiosity. The data do not allow specific determination of whether host materials for these evolved gases exist as crystalline phases at abundances less than the 1 to 2% detectable by CheMin, or whether these volatiles are also hosted in amorphous materials in the <150-μm fraction. However, the release temperatures of the gases suggest fine-grained and/or poorly crystalline materials as the hosts, as discussed below.

The CO_2 released from all four Rocknest runs comprises two major peaks, at ~400° and ~510°C, and a lower-temperature shoulder, which can be fit as two discrete releases at ~225° and ~295°C (Fig. 3). The two major CO_2 peaks together comprise >70% of the CO_2 released. The highest-temperature CO_2 release is consistent with the thermal decomposition of siderite (*19*). If this peak is due entirely to siderite decomposition, it would imply ~1 wt % siderite in the Rocknest <150-μm fraction. A second possibility is that this release evolved from the thermal decomposition of nanophase magnesite, because nanophase carbonates decompose at temperatures at least 100°C lower than 2- to 50-μm-sized particles (*17*, *20*). Calcite is not a likely candidate because its decomposition begins at 685°C, a temperature substantially higher than that of the vast majority of CO_2 released from the Rocknest <150-μm fraction. A third possibility is that the two major CO_2 peaks correspond to CO_2 chemically evolved from two mineral phases, such as siderite and magnesite, by reaction with HCl (*18*), which is observed in the Rocknest EGA (Fig. 1B), likely from decomposition of a perchlorate salt (see below). Most likely, all three factors (grain size, mineralogy, and reaction with HCl) contribute to the two major CO_2 peaks.

The concurrent evolution of CO_2 and O_2 from Rocknest suggests that organic carbon (i.e., C con-

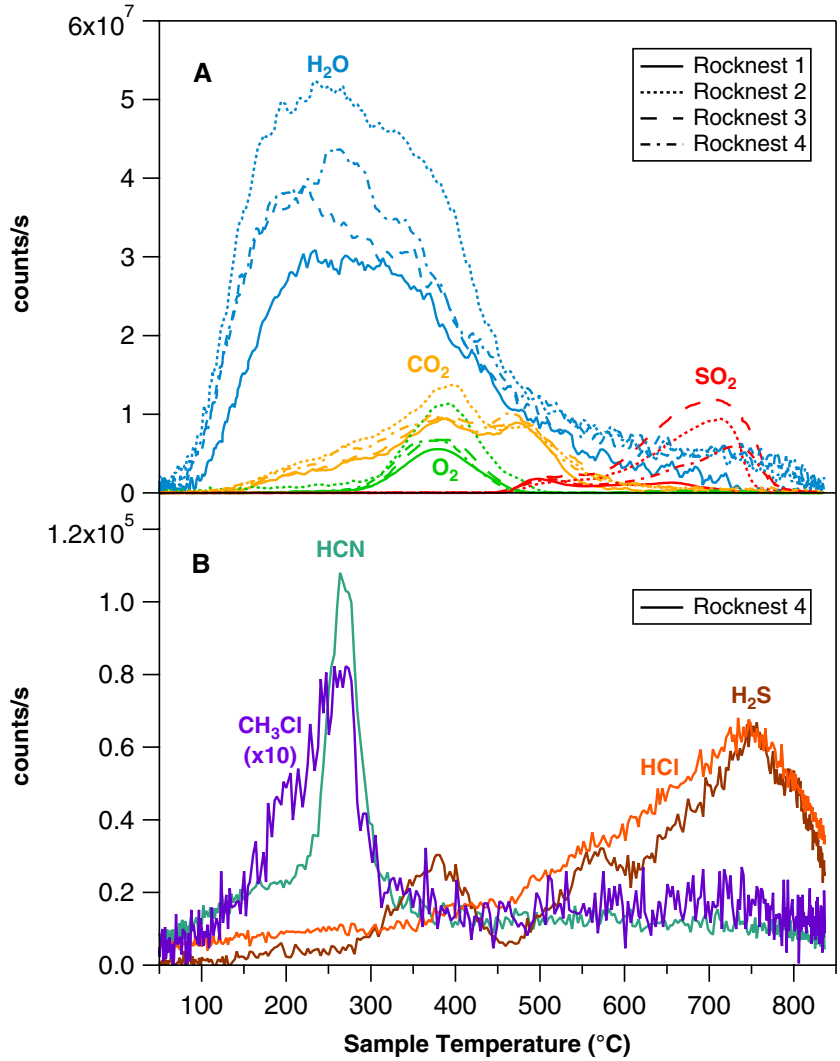

Fig. 1. Gases released from heated Rocknest aliquots. Relative abundance of molecular ions diagnostic of specific gases evolved over the 75° to 835°C pyrolysis temperature ramp. (**A**) The four most abundant gases evolved from the four Rocknest portions delivered to SAM. Major molecular ions that saturated the QMS detector were estimated on the basis of other isotopologs of that species. (**B**) Traces for *m/z* 27, 34, 36, and 52, reflecting four minor gases from the Rocknest run 4. Gas species that constitute the greatest input to the traces are labeled (27 = HCN, 34 = H_2S, 36 = HCl, and 52 = CH_3Cl), as are any scaling factors used. Minor contributions from other species are possible (e.g., the low-temperature peak of the "H_2S" trace reflects a contribution from $^{16}O^{18}O$).

tained in molecules having C, H, O, N, and/or S) oxidized within SAM is another potential CO_2 source. Such reduced carbon might be indigenous to Mars, delivered from space in the form of interplanetary dust particles and micrometeorites, or part of the instrument background. Molecular fragments from a reagent carried to Mars for use in a SAM wet chemistry experiment, MTBSTFA (*N*-methyl-*N*-*tert*-butyldimethylsilyl-trifluoroacetamide), have been identified in both empty-cup blank and Rocknest runs. A small fraction of CO_2 (<10% of the total CO_2 observed) from combustion of these organics is suggested by the amount of the most abundant MTBSTFA-related products, mono- and bi-silylated H_2O (*tert*-butyldimethylsilanol and 1,3-bis(1,1-dimethylethyl)-1,1,3,3-tetramethyldisiloxane, respectively). These sources are discussed below in conjunction with $\delta^{13}C$ measurements and organic molecular analyses.

Although the intensity and shape of traces attributable to SO_2 vary between the Rocknest samples, overall, the EGA traces indicate that SO_2 evolves from ~450° to 800°C. Two main peaks are observed, at ~500° to 550°C and ~700° to 750°C (Fig. 1). Possible sources of the evolved SO_2 include the thermal decomposition of sulfates and/or sulfites, oxidation of sulfides, and S adsorbed onto particle surfaces, which can persist to relatively high temperatures (*21*). Laboratory EGA under SAM-like conditions shows that iron sulfates produce SO_2 at temperatures consistent with Rocknest observations. Mg- and Ca-sulfates, including the anhydrite observed in Rocknest <150-μm fraction by CheMin (*15*), have SO_2 evolution temperatures too high to explain the observed SO_2. The high-temperature tail of O_2 peak at ~460°C is coincident with the initial rise of SO_2. This observation and SAM EGA detections of small amounts of H_2S, OCS, and CS_2 evolved at temperatures close to the higher-temperature SO_2 release (Fig. 1) support the hypothesis that oxidative reactions of reduced sulfur phases during heating also contributed to the evolved SO_2.

The onset of release of O_2 correlates with the release of chlorinated hydrocarbons (Fig. 1), suggesting that an oxychloride compound, such as a chlorate or perchlorate, is the source of the oxygen and chlorinated volatiles. Laboratory evaluation of various perchlorates and chlorates has not identified an unequivocal match to the SAM Rocknest data, but Ca-perchlorate provides the most reasonable match, with Fe- and Mg-bearing perchlorate, various chlorates, and mixtures with other minerals that may affect decomposition temperatures (*22*–*24*) as other possibilities.

The likely detection of an oxychloride compound by SAM is consistent with perchlorate observed in samples analyzed by the Wet Chemistry Laboratory (WCL) and the Thermal and Evolved Gas Analyzer (TEGA) instrument on the Phoenix lander (*25*), which observed a similar O_2 release during analysis of a soil sample. On the basis of WCL results, Phoenix soils were calculated to contain 0.4 to 0.6 wt % ClO_4^- (*25*). If all of the oxygen detected by SAM resulted from perchlorate decomposition, the estimated ClO_4^- abundance in the Rocknest <150-μm fraction (Table 2) would be comparable to the abundances observed by Phoenix. This abundance does not account for all of the chlorine detected by Curiosity's Alpha Particle X-ray Spectrometer (APXS) (*14*), implying the presence of other chlorine-bearing species at Rocknest.

Chlorine has been detected in every soil ever analyzed on Mars—in situ at the equatorial and mid-latitude sites of the two Viking landers (*2*) and from equator to mid-latitude by remote sensing from Mars Odyssey spacecraft (*26*). The process of perchlorate formation is believed to start with the oxidation of chlorine in gas-phase reactions in the atmosphere (*27*), various chlorine oxides produced by energetic electrons from galactic cosmic-ray interaction with the surface ice (*28*), heterogeneous mineral-catalyzed photo-oxidation of surface chlorides (*29*), or on airborne dust. The global presence of chlorine, and the detection of perchlorate in fines at two very different locations (Phoenix and Curiosity landing sites), support the hypothesis that perchlorates are globally distributed in the regolith of Mars. Perchlorates can be a sensitive marker of past climate and a potential terminal electron acceptor for martian biota. They may also form liquid brines under current martian conditions and contribute to the oxidation and transformation of martian

Table 2. Abundance of major species released upon heating of Rocknest as measured with the SAM QMS. Errors reported for molar abundances are the 2σ SD from the mean of calculations done with different *m/z* values for the same species. Weight % values were calculated with an estimated sample mass of 50 ± 8 mg (2σ), with errors propagated including the uncertainty in molar abundance (*14*).

	Molar abundances (μmol)			
	Run 1	Run 2	Run 3	Run 4
CO_2	8.3 ± 2.0	10.8 ± 2.6	10.1 ± 2.4	10.4 ± 2.5
SO_2	2.9 ± 0.2	13.7 ± 1.9	21.7 ± 2.9	10.5 ± 1.4
H_2O	43.3 ± 10.7	66.5 ± 16.2	54.5 ± 9.9	55.9 ± 11.9
O_2	3.0 ± 0.4	5.1 ± 0.6	3.7 ± 0.4	3.7 ± 0.5
	Sample weight %			
	Run 1	Run 2	Run 3	Run 4
CO_2	0.7 ± 0.2	1.0 ± 0.3	0.9 ± 0.3	0.9 ± 0.3
SO_3 equiv.	0.5 ± 0.1	2.2 ± 0.5	3.5 ± 0.7	1.7 ± 0.3
H_2O	1.6 ± 0.5	2.4 ± 0.7	2.0 ± 0.5	2.0 ± 0.5
ClO_4 equiv.	0.3 ± 0.1	0.5 ± 0.1	0.4 ± 0.1	0.4 ± 0.1

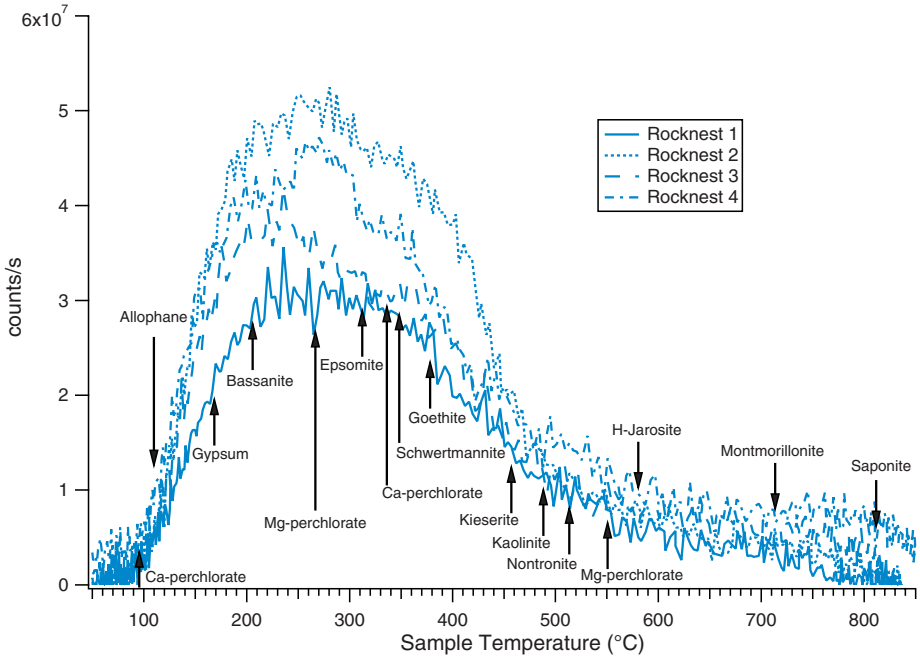

Fig. 2. Water release from Rocknest compared to laboratory measurements of mineral breakdown. Water release versus temperature for Rocknest <150-μm fraction measured by the SAM QMS. Arrows indicate temperatures of water-release peaks determined by laboratory analysis for select hydrous minerals phases under conditions similar to that in SAM (*17*).

organic matter when exposed to ionizing radiation at or near the surface or during analytical processing. Thus, a widespread presence of perchlorate salts, spatially and temporally, would have an important bearing on understanding habitability, organic matter preservation potential, and organic biosignature detection on Mars.

Isotopes

The results of the TLS isotopic analyses at Rocknest are summarized in Table 3. The strategy for the different temperature ranges of evolved gas sent to the TLS was developed with the EGA data to iteratively design experiments that selectively focused on various gas releases. For example, run 3 captured the bulk of the H_2O peak, and run 4 focused on the first of the two large CO_2 peaks. The EGA data were also used to constrain the isotopic composition of C in CO_2 and S in SO_2.

Hydrogen in all Rocknest samples is highly enriched in deuterium compared to terrestrial materials (Fig. 4), with δD values ranging from ~+3900 to +7000 per mil (‰). Run 3 should be most representative of the "bulk" of the water in Rocknest, with a value of ~+7000‰. However, significant variation in the δD value with temperature is observed, with the lower-temperature cut having the highest δD value and the highest-temperature cut having the lowest.

The δD values measured in the Rocknest <150-μm fraction are consistent with the SAM TLS measurements of water in the martian atmosphere taken before Rocknest, which show a δD value of +5000 ± 1000‰ (*30*). In addition, the Rocknest δD values are within the range of values observed by remote-sensing analysis of the martian atmosphere (*31*), where telescopic measurements from Earth have previously suggested a reservoir enriched in D by a factor of ~5 over terrestrial values. The D-enriched values in a martian soil are also consistent with D-enriched H_2O observed in both bulk (*32*) and single grains (*33*) in martian meteorites.

The close match between the δD values from H_2O in both atmospheric gas and Rocknest suggests that the H_2O-rich phases in the amorphous material were formed either in direct contact with the atmosphere or through interaction with volatiles derived from it. The variation of δD value with temperature may either record long-term variation of D/H through time or represent seasonal variations reflecting changes in the water cycle. It is likely that the water evolved at the lowest temperatures represents water in active exchange with the present atmosphere, whereas the higher-temperature releases could represent water from a more ancient time. Telescopic measurements suggest that there could be large variations in atmospheric δD value with water content of the atmosphere and season (*31*), and such variations may be reflected in the Rocknest results.

Like hydrogen in H_2O, ^{13}C-enriched CO_2 has also been observed in the atmosphere at Gale crater with SAM TLS (*30*) and QMS (*34*), with an average $\delta^{13}C$ value measured to date of ~+46‰. Unlike hydrogen, however, the CO_2-bearing phases in Rocknest soil do not fully reflect this ^{13}C-enriched atmospheric value. Rather, $\delta^{13}C$ values of CO_2 evolved from Rocknest and analyzed by TLS range from –6 to +20‰ (Table 3), and estimates of $\delta^{13}C$ over the two major CO_2 peaks using QMS data average ~+18 ± 10‰, consistent with the TLS results. These values overlap with $\delta^{13}C$ values from both carbonates and refractory/reduced carbon in martian meteorites (Fig. 5). Consistent with the above discussion of several possible CO_2 sources in SAM analyses of Rocknest, the $\delta^{13}C$ compositions likely reflect mixing of multiple carbon sources. The concurrent evolution of CO_2 and O_2 from Rocknest suggests that partial combustion of reduced carbon could contribute to evolved CO_2. $\delta^{13}C$ associated with the CO_2 release between 250° and 450°C might reflect some contribution from this combusted carbon. Previous studies of martian meteorites have shown that reduced carbon is present either as an indigenous component or from exogenous meteoritic input (*8*, *10*–*12*).

The Rocknest $\delta^{13}C$ values suggest a hint of ^{13}C enrichment, consistent with $\delta^{13}C$ values observed in martian meteorite carbonates. Specifically, the data from run 4, which most closely capture the largest CO_2 peak, has a $\delta^{13}C$ value of +20 ± 10‰, which is similar to carbonate measured in the Nakhla meteorite (*35*). This value is lower than would be expected for carbonate formed from the modern atmosphere as measured by SAM TLS (*30*). It is possible that this CO_2 release is a mixture of carbonate-derived CO_2 with a high $\delta^{13}C$ value and CO_2 depleted in ^{13}C and thus does not reflect the true carbon isotopic composition of the carbonate. It is also possible that the carbonate does have low $\delta^{13}C$ values as observed in some of the martian meteorites, suggesting that the atmosphere has changed through time (*36*). Overall, the data support a minor amount of carbonate in martian soil derived from atmosphere interaction with only transient water (*37*).

The sulfur isotopic composition of SO_2 released during run 4 was determined from QMS data at a mass-to-charge ratio (*m/z*) of 64, 65, and 66. The Rocknest <150-μm fraction, including analyses of both of the major SO_2 evolution peaks,

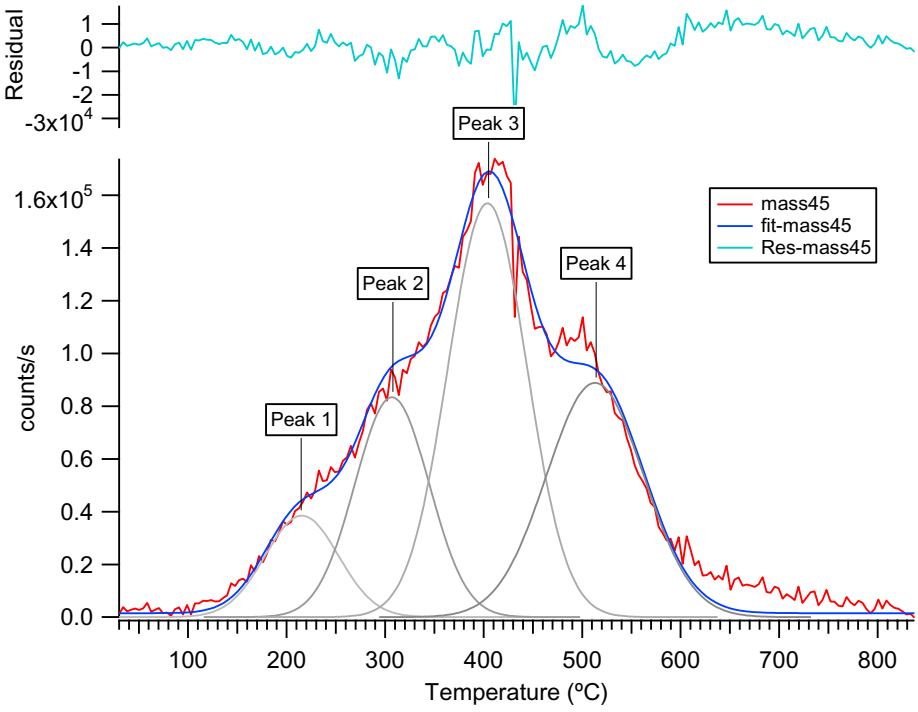

Fig. 3. Deconvolution of CO_2 release from Rocknest. Rocknest run 2 CO_2 (mass 45) versus temperature (red). Gray peaks are Gaussian fits to overall CO_2 release that sum to mass 45 fit (blue line). CO_2 fractions in each of the four peaks are 0.07, 0.22, 0.41, and 0.30, respectively.

Table 3. Isotopic composition of volatiles released upon heating of Rocknest as measured with the SAM TLS. Blank cup corrections have been applied as described in materials and methods.

Rocknest run	T range sampled (°C)	$\delta^{13}C$ in CO_2 (‰)	δD in H_2O (‰)
Run 3	234–425	–6 ± 14	7010 ± 66
Run 4	350–443	20 ± 10	4250 ± 60
Run 2	440–601	3 ± 9	3870 ± 60

have $\delta^{34}S_{VCDT}$ of 0 ± 10‰, consistent with sulfur isotopic compositions measured in martian meteorites (*38*, *39*).

Organic Matter

Chlorohydrocarbons comprising chloromethane (CH_3Cl), dichloromethane (CH_2Cl_2), trichloromethane ($CHCl_3$), and chloromethylpropene (C_4H_7Cl) were detected during SAM GC-MS analyses (Fig. 6 and Table 4). Chloromethanes detected by SAM in runs 1, 2, and 4 were at ~nanomole levels and above SAM background. Run 3 produced lower abundances of chloromethanes (typically observed at <300°C) because only a high-temperature cut of evolved gases were transferred to the GC. Minor amounts of HCN, CH_3Cl, CH_2Cl_2, and $CHCl_3$ are also observed in SAM EGA data (Fig. 1B). The abundance of these species is more than two orders of magnitude lower than that of the most abundant volatile released—H_2O.

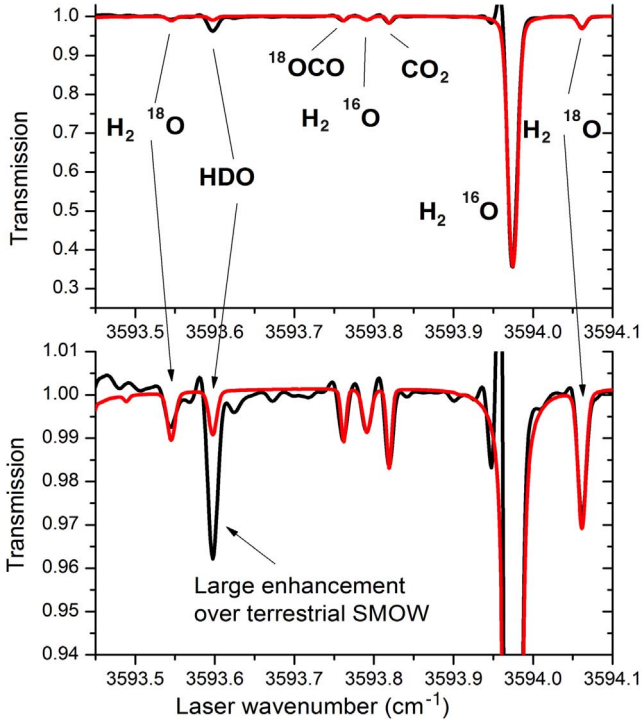

Fig. 4. Tunable laser spectrometer data showing hydrogen isotope enhancement in Rocknest. Section of a single spectrum (60 s integration) downloaded from Curiosity (black) for the Rocknest 3 sample run, showing large HDO line depth compared to calculated HITRAN spectrum (red) based on terrestrial SMOW water isotope ratios. The HDO line is ~4 times the depth of that predicted for SMOW, so that the D/H ratio is ~8 times that of SMOW, corresponding to a δD value of ~7000‰, as reported.

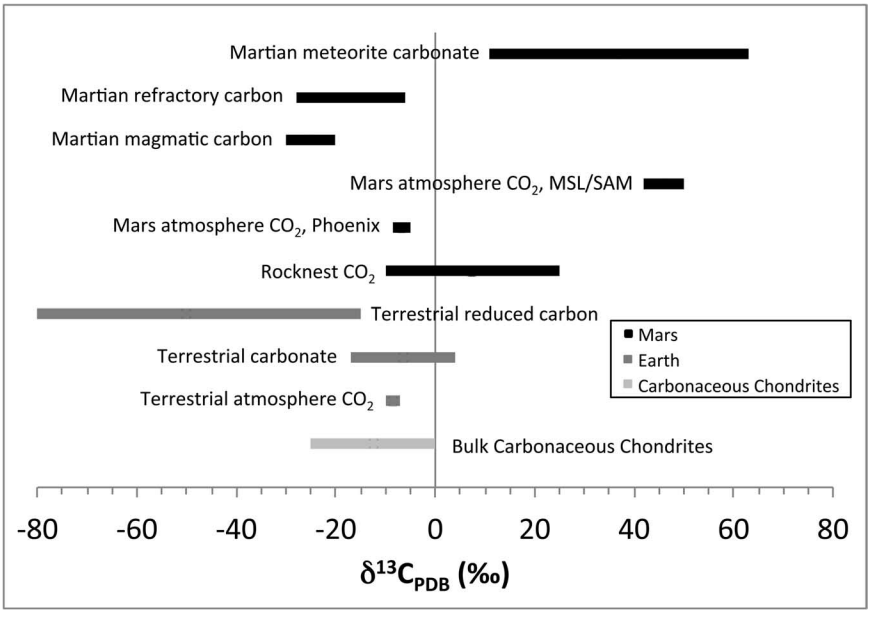

Fig. 5. Carbon isotopes in relevant solar system reservoirs. Carbon isotopic composition of materials from Mars (*44*–*46*), Earth (*47*), and carbonaceous chondrite meteorites (*48*) for comparison the values measured in Rocknest and the martian atmosphere (*30*) by the Mars Curiosity Rover.

The abundances measured by SAM are higher than the picomole levels (up to 40 parts per billion) for chloromethane and dichloromethane previously measured by the Viking pyrolysis gas chromatography–mass spectrometry (GC-MS) instruments after heating the samples of scooped fines up to 500°C (*13*). Biemann *et al.* (*13*) attribute the Viking results to chlorohydrocarbons derived from cleaning solvents used on the instrument hardware, not from the martian samples themselves. Recently, Navarro-González *et al.* (*40*) suggested that these chlorohydrocarbons may have formed by oxidation of indigenous organic matter during pyrolysis of the soil in the presence of perchlorates, but Biemann and Bada (*41*) disagree with this conclusion.

The absence of detectable chlorohydrocarbons in the SAM blank run indicates that the chlorohydrocarbons measured at Rocknest are not directly attributable to the SAM instrument background signal. However, the associated release of chloromethanes, O_2, and HCl strongly suggests that these chlorohydrocarbons are being produced within SAM by chlorination reactions involving an oxychloride compound in the Rocknest <150-μm fraction and an organic carbon precursor (*23*). Three sources for the organic carbon of this reaction are possible: (i) terrestrial sources within the SAM instrument or the Curiosity sample chain; (ii) exogenous carbon in the martian surface materials derived from infalling meteoritic carbon; and (iii) martian indigenous organic matter. A feasible explanation involves terrestrial carbon derived from the MTBSTFA, whose reaction products were identified in both the blank and soil EGA and GC analyses. On the basis of laboratory pyrolysis GC-MS experiments, pyrolytic reaction of martian Cl with organic carbon from MTBSTFA in SAM can explain the presence of the chloromethanes and chloromethylpropene detected by SAM. However, we cannot rule out the possibility that traces of organic carbon of either martian or exogenous origin contributed to some of the chlorohydrocarbons measured by SAM at Rocknest.

Overall, SAM analyses indicate that martian fines contain a number of materials with bound volatiles that can be released upon heating. These volatile-bearing materials are likely very fine-grained and associated with the amorphous component of martian regolith. The fines could be a good source of water, CO_2, and other volatiles to be leveraged by future human explorers on Mars. Isotopic compositions support an atmospheric source of the water and possibly CO_2, consistent with previously proposed formation mechanisms for carbonate and perchlorate in the fines that involve interaction with the atmosphere. Although martian organic matter was not definitively detected, the presence of materials that produce substantial amounts of oxygen upon heating suggests that detection of such compounds in martian soils will be difficult with pyrolysis techniques. The fines on Mars reveal a complex history, reflecting global, regional, and local-scale processes.

Materials and Methods

SAM Instrument Overview and Operations

The SAM instrument suite supports the MSL mission and sits inside the Curiosity rover at Gale crater on Mars. The SAM instruments are a QMS, a TLS, and a six-column GC with thermal conductivity detectors (TCDs) (*7*). These three instruments share a solid sample- and gas-processing system to generate complementary compositional and isotopic observations on each sample delivered by the rover's Sample Acquisition, Sample Processing and Handling (SA/SPaH) hardware to a SAM solid sample inlet tube or ingested directly through a gas inlet. Before each analysis, the oven for solid samples, gas-processing system, and instruments are purged with helium and heated to release any residual volatiles in the system to, in effect, precondition and clean SAM.

Scooped, sieved <150-μm-particle-size fraction, and portioned (<76 mm^3) sediments of the Rocknest aeolian drift were heated to thermally evolve gases for processing and analysis. These volatiles are the result of the following processes often happening concurrently: (i) desorption of surface-adsorbed volatiles and anions, (ii) mineral thermal decomposition, and (iii) thermochemical reactions among chemical components (*18*). When organic materials are present in solid samples, they might be desorbed at low temperatures (usually below 320°C), as is the case for small individual molecules; undergo pyrolysis (i.e., thermal bond cleavage) at higher temperatures; or contribute to thermochemical reactions (at all temperatures) (*42*).

SAM performs EGA with the QMS and isotope measurements of evolved gases with both the QMS and the TLS, with the latter being sensitive to CO_2, water, and methane (methane detection capability was not used during Rocknest runs). Organic analyses can be performed with the QMS alone or when it is coupled to the GC. SAM heated each Rocknest sample to ~835°C at a rate of 35°C/min with a He carrier gas flow rate of ~0.77 standard cm^3 per minute and at an oven pressure of ~25 mbar. The SAM QMS analyzed abundances of gases across the entire temperature range, while selected temperature ranges of the evolved gases in each run were sent to the TLS and GC for analysis (Table 1). For each portion ingested by SAM (called runs 1 through 4), the gases evolved across the selected range of temperatures were accumulated inside the TLS Herriott cell, where hydrogen isotopes in water and carbon isotopes in CO_2 were analyzed in the bulk gases. Evolved gases from a different selected temperature range sent to the GC were first captured on the hydrocarbon trap held at 5°C. The trap was subsequently heated to ~300°C under He flow, and the desorbed gases were sent to a GC channel (composed of an injection trap, MXT-CLP column, and TCD) suited for the analysis and separation of volatile organic compounds. The TCD and QMS provide detection and identification of the chemical molecules eluted from the GC.

Solid Sample Analysis Details

At Rocknest, fines from scoop #5 were delivered to SAM four times and placed in separate quartz-glass cups. The sample in each cup was flushed with pure helium (99.999%) at ~ 25 mbar at ~0.77 standard cm^3 per minute and heated at ~75°C for 15 min to release water adsorbed on mineral surfaces and minimize saturating the system with excess water. This early gas release was directly measured by the QMS. Each cup was heated in SAM oven #1 at a rate of ~35°C min^{-1} to ~835°C, where the final temperature varied slightly due to different ambient Mars environmental conditions. All evolved gases from the 75° to 835°C range were sampled by the QMS

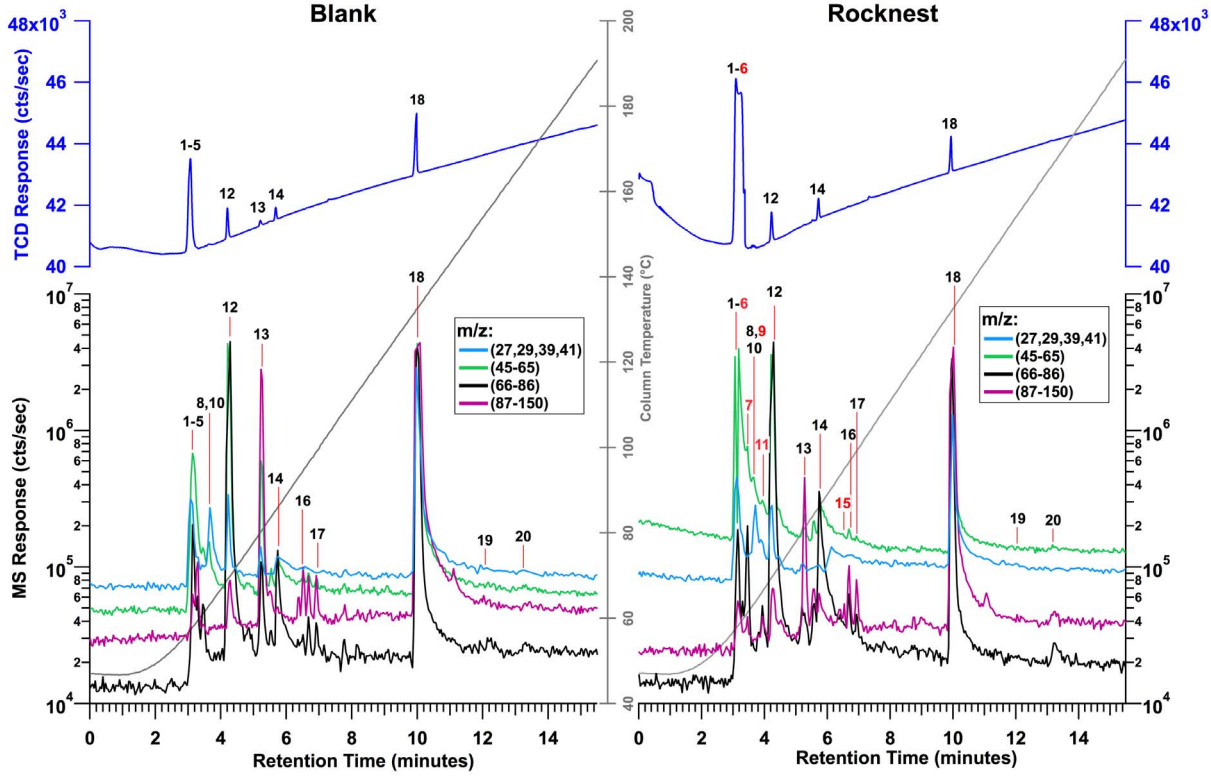

Fig. 6. Blank run and Rocknest gas chromatograph data. SAM gas chromatograph separation of volatile compounds released during the pre-Rocknest blank (left) and Rocknest run 1 (right). See materials and methods for analytical protocols. The top plots in blue show the relative intensity of the TCD signal versus GC retention time. The traces shown on the bottom plot represent peak intensities of four different scans over the specified *m/z* ranges in counts per second (cps) versus GC retention time. Key compounds (numbered) were identified by comparison to National Institute of Standards and Technology mass spectral references. The following peaks (marked in red in the Rocknest figure) were identified above measured background levels: 2, carbon dioxide; 3, sulfur dioxide; 4, hydrogen cyanide; 5, hydrogen sulfide; 6, chloromethane; 7, dichloromethane; 9, trichloromethane; 11, chloromethylpropene; 15, chlorobenzene. The following peaks are consistent with measured background levels: 1, carbon monoxide; 8, acetone; 10, acetonitrile; 12, benzene; 13, toluene; 14, *tert*-butyldimethylsilanol; 16, phenylethyne; 17, styrene; 18, 1,3-bis(1,1-dimethylethyl)-1,1,3,3-tetramethyldisiloxane; 19, trimethylsilylborate; and 20, biphenyl. See Table 4 for discussion of possible origins of each peak.

through a capillary flow restrictor. This experiment is referred to as evolved gas analysis and produced data in the form of pyrograms for individual ions defined by their *m/z* ratios. The main split of evolved gas was then passed through gas manifolds heated at 135°C to either the hydrocarbon trap for GC analysis or the TLS Herriot cell for isotopic and mixing-ratio measurements of H_2O, CO_2, or O_2, or vented to Mars. For each analytical run, different temperature cuts of gas were selected to go to the GC or TLS, but in no case was the gas sent to both at the same time. Temperature cuts for the GC and TLS are listed in Table 1.

Figures 2 and 3 show detailed analyses of the H_2O and CO_2 releases, respectively. The plot of H_2O release in Fig. 2 is generated with the QMS data from *m/z* 20, because the molecular ion for H_2O (*m/z* 18) is saturated in these runs. The release temperatures of various hydrous mineral phases marked on the plot are derived from laboratory measurements performed under conditions similar to those for the EGA in SAM. These were typically determined for single minerals, and mineral mixtures and grain-size effects can change these values. Nonetheless, the broad H_2O release peak is not clearly indicative of any one mineral phase. Figure 3 shows evolved CO_2 (*m/z* 45) as a function of temperature for Rocknest run #2, for which four discrete peaks can be fit to Gaussian peak shape to model the summed CO_2 release. The integrated areas for the fitted peaks are used to quantify the contributions from each release event to the total abundance of evolved CO_2. Although it is not possible to assign definitively specific species to each of the four peaks, oxidized organics (terrestrial or martian) and several types are carbonate are discussed in the text as likely contributing to the CO_2 peaks, especially the two major peaks.

Methods for Molar Abundance Calculations

Molar abundances were primarily computed by referencing measurements on Mars to pre-launch SAM calibration runs of quantified samples of calcite ($CaCO_3$) and a hydrated iron sulfate ($FeSO_4{\cdot}4H_2O$) (6). A calibration factor [counts per second (cps)/mol] was determined for the relevant *m/z* value in laboratory standard runs by integrating under the evolved gas curve and dividing by the number of moles evolved from the sample, assuming complete decomposition.

Under nominal SAM operating conditions, the most abundant ion of major species (e.g., *m/z* 18 for H_2O) often saturates the detector. Given a fixed detector range, this makes the instrument more sensitive to low-abundance materials. To quantify amounts with high abundances, doubly ionized molecules, ion fragments, and isotopes were used to calculate evolved gas abundances. For example, *m/z* 44 (CO_2^+) saturated the detector for most of the Rocknest runs because the amount of CO_2 evolved exceeded detector limits. To quantify the abundance of CO_2, *m/z* 12 (C^+), *m/z* 22 (CO_2^{2+}), and *m/z* 45 and 46 (isotopologs of CO_2) were used instead of *m/z* 44. The number of moles of CO_2 evolved from Rocknest samples was determined by taking an average of the total areas calculated for each *m/z* listed above. The error was calculated as 2σ SD from the mean. For H_2O, *m/z* 19 and 20 were used because *m/z* 17 and 18 were saturated, in both Rocknest and earlier laboratory calibration runs. To calculate SO_2 abundances, *m/z* 66 and 50 were used (isotopologs of SO_2 and SO) because *m/z* 64 and 48 saturated in calibration runs.

There are two additional complications encountered when calculating H_2O abundances. First, $FeSO_4{\cdot}4H_2O$ begins to lose H_2O as soon it is exposed to lower pressures, which is before the QMS begins monitoring gas evolution. Fortunately, there is a very distinct and repeatable H_2O release at slightly higher temperatures (~200°C) with a measurable mass loss. This H_2O release was used to calibrate Rocknest data. Second, Mars has a much higher D/H ratio than Earth, which can affect peak integration values, especially for *m/z* 19 (HDO). We corrected for this effect when calculating the water abundances on Mars using QMS data during EGA. The differences in the $\delta^{18}O$, $\delta^{13}C$, and $\delta^{34}S$ isotopic values between Earth and Mars are small compared to the other uncertainties involved in these abundance calculations and, therefore, were not included.

Oxygen abundance values were calculated in a slightly different way because none of the minerals run during prelaunch testing released O_2. However, a separate prelaunch characterization run was done with an equimolar gas mix of O_2, CO_2, Ar, and N_2. These data were used to determine relative calibration factors for the major atmospheric species, as discussed in Mahaffy *et al.* (*34*). Such calibration factors yield a value for relative ionization rates for O_2 and CO_2 at equivalent abundances, which were applied to the EGA data to determine calibration factors for O_2 in cps/mol.

Isotope Data Reporting Convention

All isotope results are presented in standard delta notation (δD, $\delta^{13}C$, $\delta^{34}S$) with respect to Vienna standard mean ocean water (VSMOW) for hydrogen, Vienna Pee Dee belemnite (VPDB) for carbon, and Vienna Cañon Diablo troilite (VCDT) for sulfur. Here, $\delta(‰) = [R_{meas}/R_{std} - 1] \times 1000$, where R_{meas} is the measured isotope ratio (heavy/light), and R_{std} is the ratio of the relevant reference standard.

TLS Operational Conditions and Data Reduction

TLS is a two-channel tunable laser spectrometer that uses direct and second harmonic detection of infrared laser light absorbed after multipassing a sample cell. For the results reported here, the sample cell path length is 43 passes of a ~19.5-cm cell length, or 840 cm. TLS scans over individual rovibrational lines in two spectral regions near 2.78 μm; one centered at 3590 cm^{-1} for

Table 4. Inorganic and organic volatile species detected by the SAM GC-MS upon heating of Rocknest and their possible origins. MTBSTFA (*N*-tert-butyldimethylsilyl-*N*-methyltrifluoroacetamide) and DMF (dimethylformamide) are both carried within SAM for future derivatization experiments. Tenax TA is a porous polymer adsorbent resin used to concentrate organic compounds on the SAM hydrocarbon traps. Those sources that are known to be terrestrial in origin are shown in italics. Compounds in bold are observed above measured background levels.

Peak no. from Fig. 6	Compound	Possible origin(s)
1	Carbon monoxide	Unknown
2	**Carbon dioxide**	Martian carbonates/carbon?, *MTBSTFA or DMF*
3	**Sulfur dioxide**	Martian S-bearing minerals
4	**Hydrogen cyanide**	*MTBSTFA* + perchlorate or high-T martian source?
5	**Hydrogen sulfide**	Product of S-bearing minerals
6	**Chloromethane**	*MTBSTFA* or martian carbon? + perchlorates
7	**Dichloromethane**	*MTBSTFA* or martian carbon? + perchlorates
8	Acetone	*MTBSTFA* or *DMF*
9	**Trichloromethane**	*MTBSTFA* or martian carbon? + perchlorates
10	Acetonitrile	*MTBSTFA* or *DMF*
11	**Chloromethylpropene**	*MTBSTFA* + perchlorates
12	Benzene	*Tenax TA*
13	Toluene	*Tenax TA*
14	*tert*-Butyldimethylsilanol	*MTBSTFA* + water
15	**Chlorobenzene**	HCl + Cl_2 + *Tenax TA*
16	Phenylethyne	*Tenax TA*
17	Styrene	*Tenax TA*
18	1,3-bis(1,1-dimethylethyl)-1,1,3,3-tetramethyldisiloxane	*MTBSTFA* + water
19	Trimethylsilylborate	*MTBSTFA + glass beads*
20	Biphenyl	*Tenax TA*

CO_2 isotopes, and a second centered at 3594 cm^{-1} for both CO_2 and H_2O isotopes. The lines used in both regions have no discernable interferences. In the 3594-cm^{-1} region, the CO_2 and H_2O lines used interleave across the spectrum without interference, allowing determination of isotope ratios across widely varying CO_2 and H_2O abundances in both atmospheric and evolved gas experiments. For carbon isotopes, the values given are the weighted means of two separate pairs of lines, one pair from each region. Further data-processing details and calibration are described in the supplementary materials accompanying Webster *et al*. (*30*). Figure 4 is a good example of a TLS flight spectrum used for isotope ratio measurement, showing the large enhancement of the HDO line over that expected (HITRAN database) for terrestrial water.

The TLS sample cell (Herriott cell) is first pumped out by using the SAM turbomolecular pump with empty cell pressures of CO_2 and H_2O that are insignificant compared to either EGA or "blank cup" runs. At some predetermined time during either the four EGA or single blank cup runs, temperature cuts of evolved gas are sent to the TLS (Table 1), where they produced Herriott cell pressures of 4 to 9 mbar of principally helium, with evolved water and carbon dioxide as minor components. Before the Rocknest EGA runs reported here, a blank cup run was conducted under the identical conditions (He flow, temperature cut, pressure, etc.) but without solid sample in the pyrolysis oven. Resulting signals (abundances) for CO_2 and H_2O were not large compared to the Rocknest abundance values, and isotope values are similar to those of the samples, but nonetheless it is appropriate to make a correction. This correction was weighted by the relative abundance of the gas of interest. Specifically, the H_2O abundances in the blank were ~3% of the total water measured, and the CO_2 abundances were ~5 to 10% of the total CO_2 measured in Rocknest aliquots. Blank cup values for measured $\delta^{13}C$ in CO_2 was –80‰ and δD in H_2O was 3880‰. The TLS measured results are therefore the combination of an underlying background (blank cup) contribution and the Rocknest sample contribution in proportions dependent on the relative abundances of water and carbon dioxide from each. Because the blank cup abundances of these gases is much smaller than those evolved from the Rocknest samples, the corrections to the measured isotope ratios are usually small. Given the small abundance of H_2O and CO_2 in the blank, the blank isotope values have relatively large uncertainties, and these are propagated through the correction calculation. The results given in Table 3 are the Rocknest sample isotope ratios after correction for the blank cup values.

QMS Isotope Value Calculations

Isotope ratios from QMS data obtained through EGA of solid samples are computed from the time-integrated signal at isotopologs for the compounds of interest. For CO_2, the $^{13}C/^{12}C$ ratio is determined from *m/z* 45 and 46, with correction for oxygen contributions based on the most relevant TLS measurements of the oxygen isotopic composition in CO_2. The values of $\delta^{13}C$ given in the main text were computed on the basis of an estimated $\delta^{18}O$ value of –28‰, as determined by the TLS for CO_2 released during Rocknest 4, because the gas sample sent to TLS during this run was the most representative of the peak CO_2 release from Rocknest samples. The carbon isotopic composition of CO_2 during these runs cannot be calculated from the more typical pairs of *m/z* 12-13 or 44-45 because of interference from MTBSTFA background at *m/z* 13 and detector saturation at *m/z* 44.

For SO_2, the $^{34}S/^{32}S$ ratio is computed from *m/z* 64-66, with correction for oxygen contributions (assumed $\delta^{18}O$ of 50 ± 5‰) based on TLS measurements of the oxygen isotopic composition of both CO_2 and H_2O in the martian atmosphere. For both CO_2 and SO_2, ^{17}O contributions were estimated from the assumed $\delta^{18}O$ on the basis of a $\Delta^{17}O$ of 0.32‰, the average for martian silicates (*43*).

GC-TCD and GC-MS Operational Conditions

The SAM GC hydrocarbon trap consists of three layers: nonporous silica beads, Tenax TA adsorbant (porous 2.6-diphenylene oxide polymer resin), and Carbonsieve G adsorbant (graphitized carbon) (*7*). Gases were passed through the hydrocarbon trap that had been cooled to 5°C and selectively condensed onto glass beads or adsorbed on the basis of volatility, molecular size, and chemistry. Thermal desorption at 300°C for 4 min under He (0.5 standard cm^3 per minute, 0.9 bar) released analytes from the hydrocarbon trap in the opposite direction. Analytes then collected on a Tenax TA injection trap of the GC. The injection trap was then flash heated to 300°C. All four Rocknest GC analyses used the MTX-CLP column (30-m length, 0.25-mm internal diameter, 0.25-μm film thickness), which has a polydimethylsiloxane with phenyl and cyanopropyle film (*7*) and is designed for separating mid–molecular weight hydrocarbons. The column temperature was programmed from 50° to 220°C at 10°C min^{-1} and He carrier gas was held at a constant column inlet pressure of 0.9 bar. Gases eluting from the GC were nondestructively detected by the TCD and then ionized by electron impact at 70 eV in the QMS source, which fragmented molecules in a predictable fashion. The QMS scanned for ions in a *m/z* range of 2 to 535 using the Smart Scanning algorithm previously described (*7*). The GC-TCD result is shown as a single chromatogram for all detected molecules in which the retention time (*x* axis) is normalized to the GC retention time. GC-MS results are given as individual ion chromatograms and mass spectra for isolated peaks, in which the mass spectra were generated with a custom data-processing program.

The identification of the chlorohydrocarbons in the GC-MS data was based on the retention times and comparisons of the mass fragmentation patterns to the NIST11 library. The abundances of the chlorohydrocarbon compounds (~10^{-2} to 1 nmol) were determined by comparing the fitted peaks in the Rocknest data to those of known amounts of hexane measured during preflight calibration runs on SAM GC, corrected for differences in ionization efficiency (*34*). These abundances are also corrected for the gas fraction sent to the hydrocarbon trap with EGA data (Table 1).

EGA, GC-TCD, and GC-MS Background Measurements

Within SAM, there are several common sources of organic molecules that are typical of similar, nonflight instruments. These include (i) wet chemistry reagents used for derivatization (i.e., MTBSTFA and DMF) and thermochemolysis [i.e., tetramethylammonium hydroxide in methanol (TMAH)] and their breakdown products; (ii) the Tenax TA, a porous, 2.6-diphenylene oxide polymer resin adsorbant that slowly degrades with use into benzene, toluene, tropylium ion, biphenyl, and other single–aromatic ring structures; and (iii) the polymer films inside the capillary columns that promote selective molecular separation. The molecules from these sources are known and make up what is referred to as instrument background signal, which is expected to change over the course of the SAM instrument's lifetime and is continuously monitored by analysis of empty sample cup or "blanks." Contributions of aromatics from the Tenax TA traps to TCD and QMS (post-GC) data have been determined on the basis of their absence in EGA data. The blank analysis run before Rocknest fines was the first analysis performed since prelaunch testing, and it showed the presence of DMF, MTBSTFA products, Tenax TA products, and terrestrial water (Table 4). TLS measurements of D/H in water indicated that further heating and purging of the system largely eliminated the terrestrial water.

References and Notes

1. J. Brückner, G. Dreibus, R. Rieder, H. Wanke, Refined data of Alpha Proton X-ray Spectrometer analyses of soils and rocks at the Mars Pathfinder site: Implications for surface chemistry. *J. Geophys. Res. Planets* **108**, 8094 (2003). doi: 10.1029/2003JE002060
2. B. C. Clark *et al*., Chemical composition of Martian fines. *J. Geophys. Res.* **87**, 10059 (1982). doi: 10.1029/JB087iB12p10059
3. R. Gellert *et al*., Chemistry of rocks and soils in Gusev Crater from the alpha particle x-ray spectrometer. *Science* **305**, 829–832 (2004). doi: 10.1126/science.1099913; pmid: 15297665
4. H. Wänke, J. Bruckner, G. Dreibus, R. Rieder, I. Ryabchikov, Chemical composition of rocks and soils at the pathfinder site. *Space Sci. Rev.* **96**, 317–330 (2001). doi: 10.1023/A:1011961725645
5. A. S. Yen *et al*., An integrated view of the chemistry and mineralogy of martian soils. *Nature* **436**, 49–54 (2005). doi: 10.1038/nature03637; pmid: 16001059
6. S. R. Taylor, S. M. McLennan, *Planetary Crusts: Their Composition, Origin and Evolution* (Cambridge Univ. Press, Cambridge, 2009).
7. P. R. Mahaffy *et al*., The Sample Analysis at Mars Investigation and Instrument Suite. *Space Sci. Rev.* **170**, 401–478 (2012). doi: 10.1007/s11214-012-9879-z

8. M. M. Grady, A. B. Verchovsky, I. P. Wright, Magmatic carbon in Martian meteorites: Attempts to constrain the carbon cycle on Mars. *Int. J. Astrobiol.* **3**, 117–124 (2004). doi: 10.1017/S1473550404002071
9. A. Steele *et al.*, Comprehensive imaging and Raman spectroscopy of carbonate globules from Martian meteorite ALH 84001 and a terrestrial analogue from Svalbard. *Meteorit. Planet. Sci.* **42**, 1549–1566 (2007). doi: 10.1111/j.1945-5100.2007.tb00590.x
10. A. Steele *et al.*, A reduced organic carbon component in martian basalts. *Science* **337**, 212–215 (2012). doi: 10.1126/science.1220715; pmid: 22628557
11. L. Becker, B. Popp, T. Rust, J. L. Bada, The origin of organic matter in the Martian meteorite ALH84001. *Adv. Space Res.* **24**, 477–488 (1999). doi: 10.1016/S0273-1177(99)00090-3; pmid: 11543335
12. M. A. Sephton *et al.*, High molecular weight organic matter in martian meteorites. *Planet. Space Sci.* **50**, 711–716 (2002). doi: 10.1016/S0032-0633(02)00053-3
13. K. Biemann *et al.*, The search for organic substances and inorganic volatile compounds in the surface of Mars. *J. Geophys. Res.* **82**, 4641–4658 (1977). doi: 10.1029/JS082i028p04641
14. D. F. Blake *et al.*, Curiosity at Gale crater, Mars: Characterization and analysis of the Rocknest sand shadow. *Science* **341**, 1239505 (2013).
15. D. L. Bish *et al.*, X-ray diffraction results from Mars Science Laboratory: Mineralogy of Rocknest at Gale crater. *Science* **341**, 1238932 (2013).
16. R. C. Anderson *et al.*, Collecting samples in Gale Crater, Mars; an overview of the Mars Science Laboratory Sample Acquisition, Sample Processing and Handling System. *Space Sci. Rev.* **170**, 57–75 (2012). doi: 10.1007/s11214-012-9898-9
17. D. L. Bish, C. J. Duffy, in *Thermal Analysis in Clay Science*, J. W. Stucki, D. L. Bish, Eds. (Clay Minerals Society, Boulder, CO, 1990), vol. 3, pp. 95–189.
18. K. M. Cannon, B. Sutter, D. Ming, W. V. Boynton, R. C. Quinn, Perchlorate induced low temperature carbonate decomposition in the Mars Phoenix Thermal and Evolved Gas Analyzer (TEGA). *Geophys. Res. Lett.* **39**, L13203 (2012). doi: 10.1029/2012GL051952
19. B. Sutter *et al.*, The detection of carbonate in the martian soil at the Phoenix Landing site: A laboratory investigation and comparison with the Thermal and Evolved Gas Analyzer (TEGA) data. *Icarus* **218**, 290–296 (2012). doi: 10.1016/j.icarus.2011.12.002
20. H. V. Lauer Jr., P. D. Archer, B. Sutter, P. B. Niles, D. M. Ming, in *Lunar Planet. Sci.* **43** (2012), abstr. 2299.
21. B. C. Clark, A. K. Baird, Is the Martian lithosphere sulfur rich? *J. Geophys. Res.* **84**, 8395 (1979). doi: 10.1029/JB084iB14p08395
22. R. Furuichi, T. Ishii, K. Kobayashi, Phenomenological study of the catalytic thermal decomposition of potassium perchlorate by iron(II) oxides with different preparing histories. *J. Therm. Anal.* **6**, 305–320 (1974). doi: 10.1007/BF01950062
23. D. P. Glavin *et al.*, Evidence for perchlorates and the origin of chlorinated hydrocarbons detected by SAM at the Rocknest aeolian deposit in Gale Crater. *J. Geophys. Res. Planets* (2013). doi: 10.1002/jgre.20127
24. M. M. Markowitz, D. A. Boryta, The differential thermal analysis of perchlorates. VII. Catalytic decompositions of the alkali metal perchlorates by manganese dioxide. *J. Phys. Chem.* **69**, 1114–1123 (1965). doi: 10.1021/j100888a005
25. M. H. Hecht *et al.*, Detection of perchlorate and the soluble chemistry of martian soil at the Phoenix lander site. *Science* **325**, 64–67 (2009). pmid: 19574385
26. J. M. Keller *et al.*, Equatorial and midlatitude distribution of chlorine measured by Mars Odyssey GRS. *J. Geophys. Res.* **111**, E03S08 (2006). doi: 10.1029/2006je002679
27. D. C. Catling *et al.*, Atmospheric origins of perchlorate on Mars and the Atacama. *J. Geophys. Res.* **115**, E00E11 (2010). doi: 10.1029/2009JE003425
28. Y. S. Kim, K. P. Wo, S. Maity, S. K. Atreya, R. I. Kaiser, Radiation-induced formation of chlorine oxides and their potential role in the origin of Martian perchlorates. *J. Am. Chem. Soc.* **135**, 4910–4913 (2013). doi: 10.1021/ja3122922; pmid: 23506371
29. J. D. Schuttlefield, J. B. Sambur, M. Gelwicks, C. M. Eggleston, B. A. Parkinson, Photooxidation of chloride by oxide minerals: Implications for perchlorate on Mars. *J. Am. Chem. Soc.* **133**, 17521–17523 (2011). doi: 10.1021/ja2064878; pmid: 21961793
30. C. R. Webster *et al.*, Isotope ratios of H, C, and O in CO_2 and H2O of the martian atmosphere. *Science* **341**, 260–263 (2013). doi: 10.1126/science.1237961; pmid: 23869013
31. R. E. Novak, M. J. Mumma, G. L. Villanueva, Measurement of the isotopic signatures of water on Mars; Implications for studying methane. *Planet. Space Sci.* **59**, 163–168 (2011). doi: 10.1016/j.pss.2010.06.017
32. L. A. Leshin, S. Epstein, E. M. Stolper, Hydrogen isotope geochemistry of SNC meteorites. *Geochim. Cosmochim. Acta* **60**, 2635–2650 (1996). doi: 10.1016/0016-7037(96)00122-6
33. L. A. Leshin, Insights into martian water reservoirs from analyses of martian meteorite QUE94201. *Geophys. Res. Lett.* **27**, 2017–2020 (2000). doi: 10.1029/1999GL008455
34. P. R. Mahaffy *et al.*, Abundance and isotopic composition of gases in the martian atmosphere from the Curiosity rover. *Science* **341**, 263–266 (2013). doi: 10.1126/science.1237966; pmid: 23869014
35. I. P. Wright, M. M. Grady, C. T. Pillinger, Chassigny and the nakhlites: Carbon-bearing components and their relationship to martian environmental conditions. *Geochim. Cosmochim. Acta* **56**, 817–826 (1992). doi: 10.1016/0016-7037(92)90100-W
36. P. B. Niles, W. V. Boynton, J. H. Hoffman, D. W. Ming, D. Hamara, Stable isotope measurements of martian atmospheric CO_2 at the Phoenix landing site. *Science* **329**, 1334–1337 (2010). doi: 10.1126/science.1192863; pmid: 20829484
37. J. L. Bandfield, T. D. Glotch, P. R. Christensen, Spectroscopic identification of carbonate minerals in the martian dust. *Science* **301**, 1084–1087 (2003). doi: 10.1126/science.1088054; pmid: 12934004
38. J. Farquhar, J. Savarino, T. L. Jackson, M. H. Thiemens, Evidence of atmospheric sulphur in the martian regolith from sulphur isotopes in meteorites. *Nature* **404**, 50–52 (2000). doi: 10.1038/35003517; pmid: 10716436
39. J. P. Greenwood, L. R. Riciputi, H. Y. McSween Jr., Sulfide isotopic compositions in shergottites and ALH84001, and possible implications for life on Mars. *Geochim. Cosmochim. Acta* **61**, 4449–4453 (1997). doi: 10.1016/S0016-7037(97)00246-9
40. R. Navarro-González, E. Vargas, J. de la Rosa, A. C. Raga, C. P. McKay, Reanalysis of the Viking results suggests perchlorate and organics at midlatitudes on Mars. *J. Geophys. Res.* **115**, E12010 (2010). doi: 10.1029/2010JE003599
41. K. Biemann, J. L. Bada, Comment on "Reanalysis of the Viking results suggests perchlorate and organics at midlatitudes on Mars" by Rafael Navarro-González *et al.* *J. Geophys. Res.* **116**, E12001 (2011). doi: 10.1029/2011JE003869
42. S. C. Moldoveanu, *Analytical Pyrolysis of Natural Organic Polymers* (Elsevier, Amsterdam, 1998), pp. 496.
43. I. A. Franchi, I. P. Wright, A. S. Sexton, C. T. Pillinger, The oxygen-isotopic composition of Earth and Mars. *Meteorit. Planet. Sci.* **34**, 657–661 (1999). doi: 10.1111/j.1945-5100.1999.tb01371.x
44. A. J. T. Jull, C. J. Eastoe, S. Cloudt, Isotopic composition of carbonates in the SNC meteorites, Allan Hills 84001 and Zagami. *J. Geophys. Res. Planets* **102**, 1663 (1997). doi: 10.1029/96JE03111
45. P. B. Niles, L. A. Leshin, Y. Guan, Microscale carbon isotope variability in ALH84001 carbonates and a discussion of possible formation environments. *Geochim. Cosmochim. Acta* **69**, 2931–2944 (2005). doi: 10.1016/j.gca.2004.12.012
46. I. P. Wright, R. H. Carr, C. T. Pillinger, Carbon abundance and isotopic studies of Shergotty and other shergottite meteorites. *Geochim. Cosmochim. Acta* **50**, 983–991 (1986). doi: 10.1016/0016-7037(86)90379-0
47. J. Hoefs, *Stable Isotope Geochemistry* (Springer-Verlag, Heidelberg, Germany, ed. 2, 1980).
48. M. A. Sephton, Organic compounds in carbonaceous meteorites. *Nat. Prod. Rep.* **19**, 292–311 (2002). doi: 10.1039/b103775g; pmid: 12137279

Acknowledgments: NASA provided support for the development and operation of SAM, and for the SAM Science Team, led out of NASA's Goddard Space Flight Center. The GC-TCD subsystem for SAM was developed in France, with the support of CNES. The TLS subsystem for SAM was developed at the Jet Propulsion Laboratory, California Institute of Technology, under a contract with NASA. Data from the SAM experiment are archived in the Planetary Data System (pds.nasa.gov). The SAM development, operations, and testbed teams provided essential contributions to the successful operation of SAM on Mars and the acquisition of these data.

Supplementary Materials

www.sciencemag.org/content/341/6153/1238937/suppl/DC1
MSL Science Team Author List

9 April 2013; accepted 2 August 2013
10.1126/science.1238937

Supplementary Materials for

Volatile, Isotope, and Organic Analysis of Martian Fines with the Mars Curiosity Rover

L. A. Leshin,* P. R. Mahaffy, C. R. Webster, M. Cabane, P. Coll, P. G. Conrad, P. D. Archer Jr., S. K. Atreya, A. E. Brunner, A. Buch, J. L. Eigenbrode, G. J. Flesch, H. B. Franz, C. Freissinet, D. P. Glavin, A. C. McAdam, K. E. Miller, D. W. Ming, R. V. Morris, R. Navarro-González, P. B. Niles, T. Owen, R. O. Pepin, S. Squyres, A. Steele, J. C. Stern, R. E. Summons, D. Y. Sumner, B. Sutter, C. Szopa, S. Teinturier, M. G. Trainer, J. J. Wray, J. P. Grotzinger, MSL Science Team

*Corresponding author. E-mail: leshin@rpi.edu

Published 27 September 2013, *Science* **341**, 1238937 (2013)
DOI: 10.1126/science.1238937

This PDF file includes:

Mars Science Laboratory (MSL) Science Team

Aalto University
Osku Kemppinen

Applied Physics Laboratory (APL) at Johns Hopkins University
Nathan Bridges, Jeffrey R. Johnson, Michelle Minitti

Applied Research Associates, Inc. (ARA)
David Cremers

Arizona State University (ASU)
James F. Bell III, Lauren Edgar, Jack Farmer, Austin Godber, Meenakshi Wadhwa, Danika Wellington

Ashima Research
Ian McEwan, Claire Newman, Mark Richardson

ATOS Origin
Antoine Charpentier, Laurent Peret

Australian National University (ANU)
Penelope King

Bay Area Environmental Research Institute (BAER)
Jennifer Blank

Big Head Endian LLC
Gerald Weigle

Brock University
Mariek Schmidt

Brown University
Shuai Li, Ralph Milliken, Kevin Robertson, Vivian Sun

California Institute of Technology (Caltech)
Michael Baker, Christopher Edwards, Bethany Ehlmann, Kenneth Farley, Jennifer Griffes, Hayden Miller, Megan Newcombe, Cedric Pilorget, Melissa Rice, Kirsten Siebach, Katie Stack, Edward Stolper

Canadian Space Agency (CSA)
Claude Brunet, Victoria Hipkin, Richard Léveillé, Geneviève Marchand, Pablo Sobrón Sánchez

Capgemini France
Laurent Favot

Carnegie Institution of Washington
George Cody

Carnegie Mellon University
Lorenzo Flückiger, David Lees, Ara Nefian

Catholic University of America
Mildred Martin

Centre National de la Recherche Scientifique (CNRS)
Marc Gailhanou, Frances Westall, Guy Israël

Centre National d'Etudes Spatiales (CNES)
Christophe Agard, Julien Baroukh, Christophe Donny, Alain Gaboriaud, Philippe Guillemot, Vivian Lafaille, Eric Lorigny, Alexis Paillet, René Pérez, Muriel Saccoccio, Charles Yana

Centro de Astrobiología (CAB)
Carlos Armiens-Aparicio, Javier Caride Rodríguez, Isaías Carrasco Blázquez, Felipe Gómez Gómez , Javier Gómez-Elvira, Sebastian Hettrich, Alain Lepinette Malvitte, Mercedes Marín Jiménez, Jesús Martínez-Frías, Javier Martín-Soler, F. Javier Martín-Torres, Antonio Molina Jurado, Luis Mora-Sotomayor, Guillermo Muñoz Caro, Sara Navarro López, Verónica Peinado-González, Jorge Pla-García, José Antonio Rodriguez Manfredi, Julio José Romeral-Planelló, Sara Alejandra Sans Fuentes, Eduardo Sebastian Martinez, Josefina Torres Redondo, Roser Urqui-O'Callaghan, María-Paz Zorzano Mier

Chesapeake Energy
Steve Chipera

Commissariat à l'Énergie Atomique et aux Énergies Alternatives (CEA)
Jean-Luc Lacour, Patrick Mauchien, Jean-Baptiste Sirven

Concordia College
Heidi Manning

Cornell University
Alberto Fairén, Alexander Hayes, Jonathan Joseph, Robert Sullivan, Peter Thomas

CS Systemes d'Information
Audrey Dupont

Delaware State University
Angela Lundberg, Noureddine Melikechi, Alissa Mezzacappa

Denver Museum of Nature & Science

Julia DeMarines, David Grinspoon

Deutsches Zentrum für Luft- und Raumfahrt (DLR)
Günther Reitz

eINFORMe Inc. (at NASA GSFC)
Benito Prats

Finnish Meteorological Institute
Evgeny Atlaskin, Maria Genzer, Ari-Matti Harri, Harri Haukka, Henrik Kahanpää, Janne Kauhanen, Osku Kemppinen, Mark Paton, Jouni Polkko, Walter Schmidt, Tero Siili

GeoRessources
Cécile Fabre

Georgia Institute of Technology
Mary Beth Wilhelm

Géosciences Environnement Toulouse (GET)
Franck Poitrasson

Global Science & Technology, Inc.
Kiran Patel

Honeybee Robotics
Stephen Gorevan, Stephen Indyk, Gale Paulsen

Imperial College
Sanjeev Gupta

Indiana University Bloomington
David Bish, Juergen Schieber

Institut d'Astrophysique Spatiale (IAS)
Brigitte Gondet, Yves Langevin

Institut de Chimie des Milieux et Matériaux de Poitiers (IC2MP)
Claude Geffroy

Institut de Recherche en Astrophysique et Planétologie (IRAP), Université de Toulouse
David Baratoux, Gilles Berger, Alain Cros, Claude d'Uston, Olivier Forni, Olivier Gasnault, Jérémie Lasue, Qiu-Mei Lee, Sylvestre Maurice, Pierre-Yves Meslin, Etienne Pallier, Yann Parot, Patrick Pinet, Susanne Schröder, Mike Toplis

Institut des Sciences de la Terre (ISTerre)

Éric Lewin

inXitu
Will Brunner

Jackson State University
Ezat Heydari

Jacobs Technology
Cherie Achilles, Dorothy Oehler

Laboratoire Atmosphères, Milieux, Observations Spatiales (LATMOS)
David Coscia, Guy Israël

Laboratoire de Géologié de Lyon : Terre, Planète, Environnement (LGL-TPE)
Gilles Dromart

Laboratoire de Minéralogie et Cosmochimie du Muséum (LMCM)
François Robert, Violaine Sautter

Laboratoire de Planétologie et Géodynamique de Nantes (LPGN)
Stéphane Le Mouélic, Nicolas Mangold, Marion Nachon

Laboratoire Interuniversitaire des Systèmes Atmosphériques (LISA)
Fabien Stalport, Pascaline François, François Raulin

Lightstorm Entertainment Inc.
James Cameron

Los Alamos National Lab (LANL)
Sam Clegg, Agnès Cousin, Dorothea DeLapp, Robert Dingler, Ryan Steele Jackson, Stephen Johnstone, Nina Lanza, Cynthia Little, Tony Nelson, Roger C. Wiens, Richard B. Williams

Lunar and Planetary Institute (LPI)
Andrea Jones, Laurel Kirkland, Allan Treiman

Malin Space Science Systems (MSSS)
Burt Baker, Bruce Cantor, Michael Caplinger, Scott Davis, Brian Duston, Kenneth Edgett, Donald Fay, Craig Hardgrove, David Harker, Paul Herrera, Elsa Jensen, Megan R. Kennedy, Gillian Krezoski, Daniel Krysak, Leslie Lipkaman, Michael Malin, Elaina McCartney, Sean McNair, Brian Nixon, Liliya Posiolova, Michael Ravine, Andrew Salamon, Lee Saper, Kevin Stoiber, Kimberley Supulver, Jason Van Beek, Tessa Van Beek, Robert Zimdar

Massachusetts Institute of Technology (MIT)
Katherine Louise French, Karl Iagnemma

Max Planck Institute for Solar System Research
Fred Goesmann, Walter Goetz, Stubbe Hviid

Microtel
Micah Johnson, Matthew Lefavor, Eric Lyness

Mount Holyoke College
Elly Breves, M. Darby Dyar, Caleb Fassett

NASA Ames
David F. Blake, Thomas Bristow, David DesMarais, Laurence Edwards, Robert Haberle, Tori Hoehler, Jeff Hollingsworth, Melinda Kahre, Leslie Keely, Christopher McKay, Mary Beth Wilhelm

NASA Goddard Space Flight Center (GSFC)
Lora Bleacher, William Brinckerhoff, David Choi, Jason P. Dworkin, Melissa Floyd, James Garvin, Daniel Harpold, Andrea Jones, David K. Martin, Alexander Pavlov, Eric Raaen, Michael D. Smith, Florence Tan

NASA Headquarters
Michael Meyer, Arik Posner, Mary Voytek

NASA Jet Propulsion Laboratory (JPL)
Robert C, Anderson, Andrew Aubrey, Luther W. Beegle, Alberto Behar, Diana Blaney, David Brinza, Fred Calef, Lance Christensen, Joy A. Crisp, Lauren DeFlores, Bethany Ehlmann, Jason Feldman, Sabrina Feldman, Joel Hurowitz, Insoo Jun, Didier Keymeulen, Justin Maki, Michael Mischna, John Michael Morookian, Timothy Parker, Betina Pavri, Marcel Schoppers, Aaron Sengstacken, John J. Simmonds, Nicole Spanovich, Manuel de la Torre Juarez, Ashwin R. Vasavada, Albert Yen

NASA Johnson Space Center (JSC)
Francis Cucinotta, John H. Jones, Elizabeth Rampe

Nolan Engineering
Thomas Nolan

Oregon State University
Martin Fisk

Piezo Energy Technologies
Leon Radziemski

Planetary Science Institute
Bruce Barraclough, Steve Bender, Daniel Berman, Eldar Noe Dobrea, Robert Tokar, David Vaniman, Rebecca M. E. Williams, Aileen Yingst

Princeton University
Kevin Lewis

Retired
Timothy Cleghorn, Wesley Huntress, Gérard Manhès

Salish Kootenai College
Judy Hudgins, Timothy Olson, Noel Stewart

Search for Extraterrestrial Intelligence Institute (SETI I)
Philippe Sarrazin

Smithsonian Institution
John Grant, Edward Vicenzi, Sharon A. Wilson

Southwest Research Institute (SwRI)
Mark Bullock, Bent Ehresmann, Victoria Hamilton, Donald Hassler, Joseph Peterson, Scot Rafkin, Cary Zeitlin

Space Research Institute
Fedor Fedosov, Dmitry Golovin, Natalya Karpushkina, Alexander Kozyrev, Maxim Litvak, Alexey Malakhov, Igor Mitrofanov, Maxim Mokrousov, Sergey Nikiforov, Vasily Prokhorov, Anton Sanin, Vladislav Tretyakov, Alexey Varenikov, Andrey Vostrukhin, Ruslan Kuzmin

Space Science Institute (SSI)
Benton Clark, Michael Wolff

State University of New York (SUNY) Stony Brook
Scott McLennan

Swiss Space Office
Oliver Botta

TechSource
Darrell Drake

Texas A&M
Keri Bean, Mark Lemmon

The Open University
Susanne P. Schwenzer

United States Geological Survey (USGS) Flagstaff
Ryan B. Anderson, Kenneth Herkenhoff, Ella Mae Lee, Robert Sucharski

Universidad de Alcalá
Miguel Ángel de Pablo Hernández, Juan José Blanco Ávalos, Miguel Ramos

Universities Space Research Association (USRA)
Myung-Hee Kim, Charles Malespin, Ianik Plante

University College London (UCL)
Jan-Peter Muller

University of Alabama
Ryan Ewing

University of Arizona
William Boynton, Robert Downs, Mike Fitzgibbon, Karl Harshman, Shaunna Morrison

University of California Berkeley
William Dietrich, Onno Kortmann, Marisa Palucis

University of California Davis
Amy Williams

University of California San Diego
Günter Lugmair

University of California San Francisco
Michael A. Wilson

University of California Santa Cruz
David Rubin

University of Colorado Boulder
Bruce Jakosky

University of Copenhagen
Tonci Balic-Zunic, Jens Frydenvang, Jaqueline Kløvgaard Jensen, Kjartan Kinch, Asmus Koefoed, Morten Bo Madsen, Susan Louise Svane Stipp

University of Guelph
Nick Boyd, John L. Campbell, Ralf Gellert, Glynis Perrett, Irina Pradler, Scott VanBommel

University of Hawai'i at Manoa
Samantha Jacob, Scott Rowland

University of Helsinki
Evgeny Atlaskin, Hannu Savijärvi

University of Kiel
Eckart Boehm, Stephan Böttcher, Sönke Burmeister, Jingnan Guo, Jan Köhler, César Martín García, Reinhold Mueller-Mellin, Robert Wimmer-Schweingruber

University of Leicester
John C. Bridges

University of Maryland
Timothy McConnochie

University of Maryland Baltimore County
Mehdi Benna

University of Maryland College Park
Hannah Bower

University of Massachusetts
Hannah Blau, Thomas Boucher, Marco Carmosino

University of Michigan Ann Arbor
Harvey Elliott, Douglas Halleaux, Nilton Rennó, Michael Wong

University of New Brunswick
Beverley Elliott, John Spray, Lucy Thompson

University of New Mexico
Suzanne Gordon, Horton Newsom, Ann Ollila, Joshua Williams

University of Queensland
Paulo Vasconcelos

University of Saskatchewan
Jennifer Bentz

University of Southern California (USC)
Kenneth Nealson, Radu Popa

University of Tennessee Knoxville
Linda C. Kah, Jeffrey Moersch, Christopher Tate

University of Texas at Austin
Mackenzie Day, Gary Kocurek

University of Washington Seattle
Bernard Hallet, Ronald Sletten

University of Western Ontario
Raymond Francis, Emily McCullough

University of Winnipeg
Ed Cloutis

Utrecht University
Inge Loes ten Kate

Vernadsky Institute
Ruslan Kuzmin

Washington University in St. Louis (WUSTL)
Raymond Arvidson, Abigail Fraeman, Daniel Scholes, Susan Slavney, Thomas Stein, Jennifer Ward

Western University
Jeffrey Berger

York University
John E. Moores